Resistivity-induced coupling between voltage distribution and vibrations in dielectric elastomers

Emil Garnell, Corinne Rouby, Olivier Doaré

IMSIA, CNRS, ENSTA Paris, EDF, CEA, Institut Polytechnique de Paris, France

E-mail: emil.garnell@ensta-paris.fr,corinne.rouby@ensta-paris.fr, olivier.doare@ensta-paris.fr

Abstract. Dielectric elastomers are soft actuators made of a thin layer of elastomer sandwiched between compliant electrodes. Because of the resistivity of the electrodes, the voltage is not uniform on the actuator at high frequencies. We present experimental evidence that the voltage spatial distribution is coupled to the membrane vibrations, as well as a model based on Maxwell's equations in a moving frame to explain the coupling. The model is validated experimentally, and is used to explain the physics of the observed coupling. As a result, information on the membrane deformation can be inferred from voltage measurements, which opens self-sensing possibilities at high frequencies.

Keywords: Dielectric elastomers, Resistivity, Electrodynamics

1. Introduction

Dielectric elastomers (DEs) are soft active materials capable of large deformations under electric actuation [1]. Because of their high energy density, large achievable strain, and combined actuation and sensing possibilities, they have been considered for many applications, including artificial muscles, soft robotics, wearable sensors, loudspeakers, etc. They consist of a soft elastomeric material (typically silicone or acrylic), sandwiched between flexible electrodes. When a high voltage is applied between the electrodes, the membrane is squeezed by the Maxwell electrostatic pressure, thins down and expands in area due to incompressibility. Deformations up to 500% area strain can be reached [2].

Self-sensing can be implemented with DE actuators: the deformation of the actuator is monitored during actuation without any added sensor, by measuring the voltage and current flowing through the device. Self-sensing improves the performance of DE actuators, as they can be operated in closed loop to compensate for their limitations, such as viscoelastic creep [3].

In order to set-up self-sensing strategies, the relation between the deformation of the device and its electrical behavior must be known. At low frequencies, the DE membrane behaves as a capacitor, so measuring the capacitance, which is proportional to the membrane area, provides a good estimation of the device geometry. To measure the capacitance, a high frequency signal can be superimposed to the low frequency actuation voltage [4, 5], or the actuation signal can be directly used for sensing [6].

When the frequency increases, effects due to the electrode resistivity come into play. Combined with the capacitive nature of the DE membrane, the resistive electrodes form a resistor-capacitor circuit, which is characterized by its time constant τ_e. For frequencies higher than $1/\tau_e$, the effective voltage which actuates the transducer is smaller than the supplied voltage, leading to a decrease in performance. The resistive effects have first been modeled by lumped parameters [7, 8], and lumped models are extensively used to study self-sensing applications for one-degree-of-freedom (1-DOF) systems [9, 3].

Another resistivity-induced effect arises at higher frequencies: the voltage will no longer be uniform on the electrodes. The lumped models then fail in predicting the electrical behavior of the system, and transmission line models which account for the spatial variation of the voltage on the electrodes have been proposed as a refinement [10, 11, 12, 13], either to study the voltage distribution on DE membranes for actuator applications, or to investigate self-sensing of stacked DE transducers where the resistivity of the electrodes connections is large [14, 15]. In all these studies on the spatial distribution of the voltage on the electrodes, the influence of the dynamics of the device are neglected. This is valid for most applications, where actuation occurs at timescales which are much larger than τ_e, so the electrical behavior of the device can be computed assuming that the geometry is static.

However, this no longer holds for high frequency applications such as DEA-driven acoustics, or when the electrode resistivity is high. Only very few studies investigated the influence of the device dynamics on the electrical behavior [16, 17, 15]. These studies analysed 1-DOF systems using a lumped electrical model, but to the author's knowledge, the coupling between the voltage spatial distribution and the membrane dynamics has not been investigated neither experimentally nor numerically. The goal of this article is thus to propose a modelling approach that takes into account this coupling and present experimental results that assess the interest of such an approach. The focus will be on high frequency applications where DE devices operate at small deformations, which is the case for DE loudspeakers for example.

The article is organized as follows: in section 2, it is observed experimentally that the voltage on the electrodes of a DE actuator can be influenced by its vibrations. The rest of the paper is dedicated to modelling and understanding the physics of this coupling between the electrodynamic loading of a DE membrane and its movement: a model describing the voltage distribution on moving resistive DE devices is presented for an arbitrary geometry in section 3, and is then validated by experiments in section 4 for the inflated DE membrane configuration considered in section 2. The coupling mechanism and its consequences are finally discussed in section 5.

2. Experimental observation

In this section, it is shown experimentally that the voltage on the electrodes of DE actuators can be influenced by the displacement and the vibrations of the device.

We consider the actuator shown in figure 1(a), namely an axisymmetric DE membrane inflated over a closed cavity. This system can be actuated at high frequency, as no additional mass apart from the DE membrane is moving. It has been investigated by several researchers for use as pumps [18] or loudspeakers [19, 20, 21, 22].

The membrane is made of 50 µm-thick silicone (Elastosil Film 2030 from Wacker Chemie AG). A small prestretch of 1.1 is applied by a circular pre-stretcher [23] to keep the membrane flat during the pad-printing of the electrodes, which are made of carbon-black (Ketjenblack EC-600JD from Akzo Nobel N.V) loaded

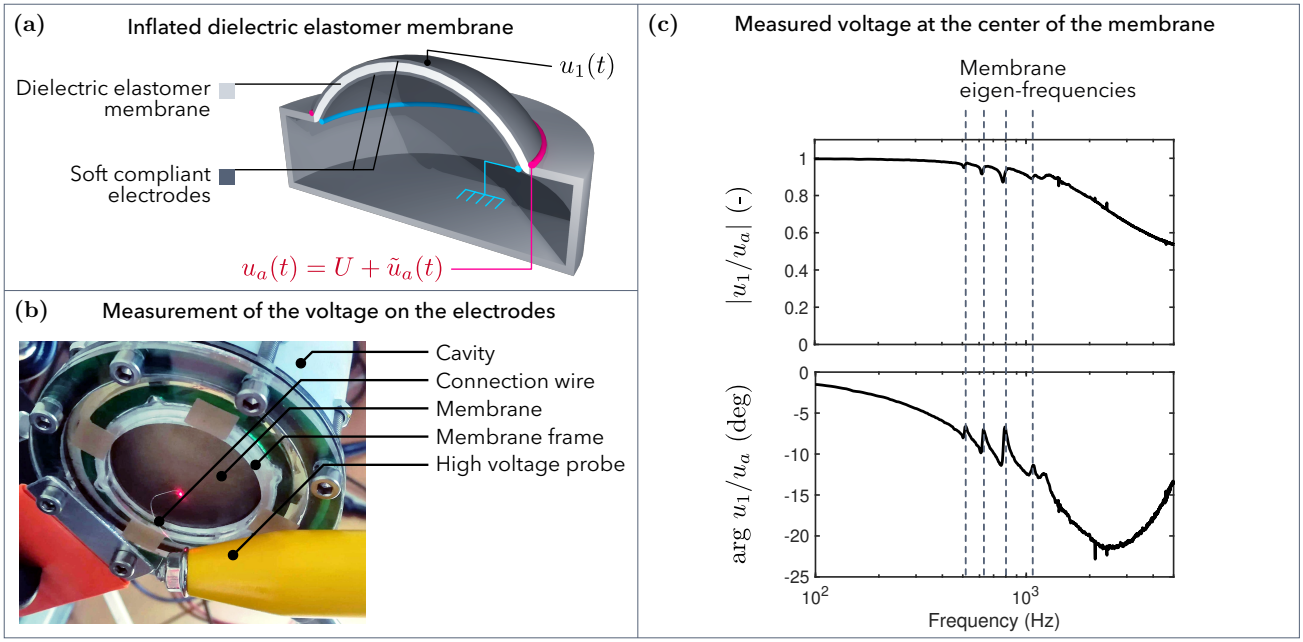

Figure 1. **(a)** Studied device: an axisymmetric dielectric elastomer membrane is inflated over a closed cavity. A biased non-stationary voltage $u_a(t) = U + \tilde{u}_a(t)$ is applied at the top electrode border. **(b)** The voltage at the center of the membrane is measured using a high voltage probe, connected to the electrodes by a thin flexible wire. **(c)** The voltage drops at eigenfrequencies of the membrane, exhibiting a coupling between the membrane dynamics and the voltage distribution.

silicone (Silbione LSR 4305 from Elkem Silicones), following the process described by Rosset *et al* [23]. As this article focuses on resistivity effects, the electrode surface resistivity is voluntarily made high around 250 kΩ/□, so that the observed resistivity-related effects are clearly visible at medium frequencies. The electrode surface resistivity is estimated by adjusting the model which is presented in the following sections on impedance measurements, so that the experimental high frequency behavior is correctly described (see figure 5). The electrode thickness is considered constant and is estimated from the added mass. The parameters of the studied prototype are given in Table 1.

The membrane is driven by a high voltage $u_a(t)$ consisting of a DC bias and a non-stationary part $u_a(t) = U + \tilde{u}_a(t)$, applied at the outer radius of the top electrode using a multifunction NI card and a Trek 609E-6 high voltage amplifier. The DC bias is $U = 1500\,\mathrm{V}$, and the oscillating part is a white noise of amplitude $|\tilde{u}_a| = 20\,\mathrm{V}$. The bottom electrode is grounded on its outer perimeter, as shown in figure 1(a). The voltage on the top electrode u_1 is measured using a high voltage probe (Testec model TT-HVP15 HF) [see figure 1(b)], and the transfer function between u_1 and u_a is computed and plotted in figure 1(c).

The voltage on the top electrode decreases at high frequencies down to half of the applied voltage, as a consequence of electrode resistivity. The electric charges are slowed down by resistivity, and do not have the time to spread on the electrodes during one period of the excitation voltage, so the electrostatic equilibrium is not satisfied, and the voltage is lower further away from the connections. The experimental observation reported here confirms the numerical predictions found in the literature [12, 24].

What is more, at the first membrane eigenfrequencies in the range 500-1200 Hz, clear peaks and drops are visible in the voltage measured on the electrode. This highlights a coupling between the membrane vibrations and the voltage distribution, which arises because of the electrode resistivity. Indeed, with perfectly conductive electrodes, the voltage would be the same on the whole electrode: $|u_1/u_a| = 1$, $\forall R$, and the membrane dynamics would not affect the voltage.

This coupling has not been studied before, and is considered in the present article because it allows information on the membrane dynamics to be retrieved from voltage measurements. It will be investigated in depth in the rest of the article, first by introducing a model describing the voltage distribution on moving resistive DE devices, validating this model, and finally discussing the physics that lie behind the observed phenomenon.

3. Model of moving resistive DEs

3.1. Studied system

In order to obtain the equations governing the voltage distribution on the electrodes of moving resistive DE devices, we consider a DE membrane on which an electrode is deposited on both sides, on the surface Σ. This setup is described in figure 2. The voltage on the top and bottom electrodes are denoted u_1 and u_2 respectively. The top electrode is connected to the voltage supply on the contour Γ_1 where the voltage is fixed at u_a. The bottom electrode is connected to the ground on Γ_2. On the rest of the border $\Gamma = \partial\Sigma$, no current is flowing out. The electrode resistivity is denoted r_e, the membrane dielectric permittivity ϵ, the membrane and electrodes thicknesses h and h_e respectively.

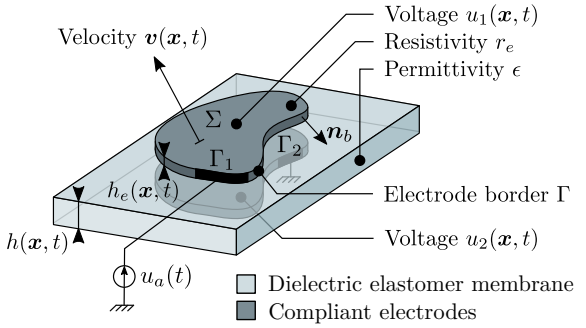

Figure 2. Studied dielectric elastomer membrane, and definition of the variables.

The electrostatic excitation which is responsible for the actuation is commonly described for incompressible DE actuators by a pressure applied on the membrane surface [1] which reads:

$$p_{\mathrm{ES}} = \epsilon \left(\frac{u_1 - u_2}{h} \right)^2 , \tag{1}$$

so to compute the behavior of the DE actuator, it is necessary to estimate precisely the distribution of the voltages u_1 and u_2.

The equations governing the voltage distribution on the electrodes will be obtained by two different methods: first by using the transmission line theory, which is the method chosen by most authors who investigate resistivity effects on DEs, and second starting directly from Maxwell's equations, and simplifying them to a moving DE membrane geometry. The two methods are finally compared to each other.

3.2. Transmission line model

Transmission line theory is an intuitive way to derive the equations governing the charge and voltage distribution on a DE actuator [12]. An element of the DE membrane is modelled as a capacitor connected to resistors which stand for the electrode resistivity, see figure 3.

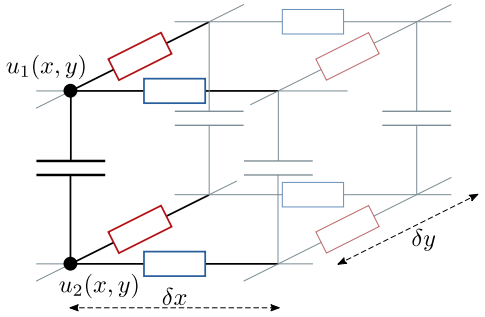

Figure 3. Transmission line model of a dielectric elastomer membrane. The black lines denote a unit cell, and the grey lines other cells. The capacitor value is $C = \frac{\epsilon}{h}\delta x \delta y$, the blue resistor values $R_x = \frac{r_e}{h_e}\frac{\delta x}{\delta y}$, and the red resistors values are $R_y = \frac{r_e}{h_e}\frac{\delta y}{\delta x}$.

Writing the current balance at the two nodes identified by dots in figure 3, and using the standard constitutive equations for resistors and capacitors, the following system of equations is obtained :

$$\boldsymbol{\nabla}_s \cdot \left(\frac{h_e}{r_e} \boldsymbol{\nabla}_s u_1 \right) = \frac{\partial}{\partial t} \left(\frac{\epsilon}{h} (u_1 - u_2) \right) , \tag{2a}$$

$$-\boldsymbol{\nabla}_s \cdot \left(\frac{h_e}{r_e} \boldsymbol{\nabla}_s u_2 \right) = \frac{\partial}{\partial t} \left(\frac{\epsilon}{h} (u_1 - u_2) \right) , \tag{2b}$$

where $\boldsymbol{\nabla}_s$ denotes the surface del operator:

$$\boldsymbol{\nabla}_s = \frac{\partial}{\partial x}\boldsymbol{e}_x + \frac{\partial}{\partial y}\boldsymbol{e}_y . \tag{3}$$

These governing equations must be completed with the following boundary conditions:

$$u_1 = u_a \qquad \text{on } \Gamma_1 , \tag{4a}$$

$$u_2 = 0 \qquad \text{on } \Gamma_2 , \tag{4b}$$

$$\boldsymbol{\nabla}_s u_1 \cdot \boldsymbol{n}_b = 0 \qquad \text{on } \Gamma \backslash \Gamma_1 , \tag{4c}$$

$$\boldsymbol{\nabla}_s u_2 \cdot \boldsymbol{n}_b = 0 \qquad \text{on } \Gamma \backslash \Gamma_2 , \tag{4d}$$

where $\boldsymbol{n}_b$ is the normal vector to the border Γ, see figure 2.

Even if it is not always written in this partial differential equation form, the system (2) with the boundary conditions (4) has been used by many authors to study resistivity effects on DEs (see [12, 24, 11] for example). Most of the time these equations are used in a more simple form, which is obtained if the thickness and resistivity are assumed to be uniform, and if the membrane thickness does not depend on time:

$$\boldsymbol{\nabla}_s^2 \bar{u} = \frac{2 r_e \epsilon}{h_e h} \frac{\partial \bar{u}}{\partial t} , \tag{5}$$

where $\bar{u} = u_1 - u_2$. This is a diffusion equation which is easily solved by finite element methods for example. Although the governing equation is more compact in the form (5), the form (2) is more practical because the boundary conditions are much easier to implement when the two variables u_1 and u_2 are used.

3.3. Maxwell model for a moving medium

The assumptions that lie behind the transmission line theory must be clarified for a moving medium. A DE membrane under dynamic excitation will move and deform, and the motion could very likely interact with the charge diffusion. In this section the equations governing the voltage distribution on the electrodes are obtained from Maxwell's equations written for a moving medium [25]. We will show that it leads to additional terms in the equations compared to the transmission line model.

Maxwell's equations for a moving medium have been written thoroughly by Kovetz [25]. Two frames are defined: $\mathcal{R}$ is a Galilean reference frame, and $\mathcal{R}'$ is the frame of reference of the matter. The frame $\mathcal{R}'$ moves relatively to $\mathcal{R}$ in a motion defined by the velocity field $\boldsymbol{v}(\boldsymbol{x}, t)$. Quantities will be noted with an apostrophe when referring to the frame $\mathcal{R}'$ and without when referring to the frame $\mathcal{R}$. In particular, the current density $\boldsymbol{i}$ refers to the velocity of the charges with respect to the reference frame $\mathcal{R}$ while the current density $\boldsymbol{i}' = \boldsymbol{i} - \rho\boldsymbol{v}$ refers to the velocity of the charges with respect to the matter. In the frame $\mathcal{R}$, Maxwell's equations for electro-quasistatics [26] read:

$$\boldsymbol{\nabla} \cdot \boldsymbol{D} = \rho \,, \tag{6a}$$

$$\boldsymbol{\nabla} \cdot \boldsymbol{i} + \frac{\partial \rho}{\partial t} = 0 \,, \tag{6b}$$

$$\boldsymbol{E} = -\boldsymbol{\nabla} u \,, \tag{6c}$$

$$\boldsymbol{D} = \epsilon_0 \boldsymbol{E} + \boldsymbol{P} \,, \tag{6d}$$

where $\boldsymbol{D}$ is the electric displacement, $\boldsymbol{E}$ the electric field, ρ the charge density, u a scalar potential from which the electric field $\boldsymbol{E}$ derives, $\boldsymbol{P}$ the polarization, and ϵ_0 the vacuum permittivity. All fields have the same expression in $\mathcal{R}$ and in $\mathcal{R}'$, except the current density $\boldsymbol{i}$.

These equations must be completed by constitutive relations between the polarization $\boldsymbol{P}'$, the current $\boldsymbol{i}'$, and the electric field $\boldsymbol{E}'$, which are written in the frame $\mathcal{R}'$ attached to the matter. In the present case two types of materials are considered:

- The membrane is made of a linear dielectric material, which does not conduct free charges, that is $\boldsymbol{i}' = 0$, and in which the polarization $\boldsymbol{P}'$ is proportional to the electric field $\boldsymbol{E}'$. Given that there are no free charges initially in the dielectric, and that there are no currents, the charge remains null at all times ($\forall t, \rho' = 0$). So in the dielectric membrane:

$$\boldsymbol{P} = \epsilon_0 \chi \boldsymbol{E} \,, \qquad \boldsymbol{i} = 0 \,, \tag{7}$$

  where χ is the membrane electric susceptibility.
- The electrodes are made of linear conductive material, which satisfies Ohm's law $\boldsymbol{i}' = \boldsymbol{E}'/r_e$, and is not polarizable, that is $\boldsymbol{P}' = 0$. Thus, in the electrodes:

$$\boldsymbol{P} = \boldsymbol{0} \,, \qquad \boldsymbol{i} - \rho\boldsymbol{v} = \frac{1}{r_e}\boldsymbol{E} \,. \tag{8}$$

Because of the thinness of the system, it is possible to describe the problem by equations written on a given reference surface Σ close to the membrane geometry, involving only two spatial variables, and not by volume equations. The construction of the 2D model is based on the following assumptions:

- In the electrodes the electric field is tangential.
- In the membrane the electric field is dominated by the normal component (fringe effects are neglected).
- Outside of the electrodes and of the membrane the electric field is null.

The first assumption amounts to assume that the potential u from which the electric field derives by Eq. (6c) does not depend on the normal direction in the electrodes.

The second assumption implies that in the membrane the electric field is expressed as a function of the electrode potentials as:

$$\boldsymbol{E} = -\frac{u_1 - u_2}{h}\boldsymbol{n} \,. \tag{9}$$

Indeed, due to the aether relation (6d) and the constitutive law (7), the electric field and the electric displacement are proportional:

$$\boldsymbol{D} = \epsilon \boldsymbol{E} \,, \tag{10}$$

where $\epsilon = \epsilon_0(1 + \chi_e)$ is the permittivity of the membrane's material. Therefore, as there are no free charges in the membrane ($\rho = 0$), Gauss's law (6a) implies that the dominant normal component of the electric field is uniform in the thickness of the membrane, and the expression (9) is finally obtained from (6c). Note that in this expression, the tangential component of the electric field has been omitted because it is negligible compared to the normal component. The tangential component is actually of the same order of magnitude in the membrane and in the electrodes, due to its continuity across the

interface between the two materials. On the other hand, our assumptions violate the continuity of the normal component of the electric field (null in the electrodes and given by Eq. (9) in the membrane). In practice, the charges will be mainly localized near the interface because of the discontinuity of the material properties, which justifies the jump of the electric field.

The charge balance (6b), Gauss's law (6a) and Ohm's law (8) are integrated in the thickness of the top electrode, to obtain surface conservation equations (see appendix Appendix A for the details):

$$\boldsymbol{\nabla}_s \cdot \boldsymbol{j}_1 + \frac{\partial \sigma}{\partial t} = 0 \,, \tag{11}$$

$$\sigma = \frac{\epsilon}{h}\left(u_1 - u_2\right) \,, \tag{12}$$

$$\boldsymbol{j}_1 - \boldsymbol{v}_{1\parallel}\sigma + \gamma_1 \boldsymbol{\nabla}_s u_1 = 0 \,, \tag{13}$$

where $\boldsymbol{j}_1$ is the surface current in the top electrode, $\boldsymbol{v}_{1\parallel}$ the tangential velocity in the top electrode, γ_1 the surface conductivity of the top electrode, σ the surface charge of the top electrode, and $\boldsymbol{\nabla}_s$ stands for the surface del operator defined by Eq. (3), where x and y now denote curvilinear coordinates on the reference surface.

By inserting in the charge balance (11) the expression of the surface current $\boldsymbol{j}_1$ given by Ohm's law (13) and the expression of the surface charge σ given by equation (12), a diffusion equation governing the voltage distribution on the top electrode is obtained, and this procedure is repeated for the bottom electrode, yielding:

$$\begin{aligned}\boldsymbol{\nabla}_s \cdot (\gamma_1 \boldsymbol{\nabla}_s u_1) =& \frac{\partial}{\partial t}\left(\frac{\epsilon}{h}(u_1 - u_2)\right) \\ &+ \boldsymbol{\nabla}_s \cdot \left(\frac{\epsilon}{h}(u_1 - u_2)\boldsymbol{v}_{1\parallel}\right) \,, \end{aligned} \tag{14a}$$

$$\begin{aligned}-\boldsymbol{\nabla}_s \cdot (\gamma_2 \boldsymbol{\nabla}_s u_2) =& \frac{\partial}{\partial t}\left(\frac{\epsilon}{h}(u_1 - u_2)\right) \\ &+ \boldsymbol{\nabla}_s \cdot \left(\frac{\epsilon}{h}(u_1 - u_2)\boldsymbol{v}_{2\parallel}\right) \,. \end{aligned} \tag{14b}$$

On the portion of the top electrode border where there is no connection, the boundary condition read $\boldsymbol{i}' \cdot \boldsymbol{n}_b = 0$, that is:

$$\boldsymbol{i} \cdot \boldsymbol{n}_b = \rho \boldsymbol{v} \cdot \boldsymbol{n}_b \qquad \text{for } \boldsymbol{x} \in \Gamma \backslash \Gamma_1 \,. \tag{15}$$

Integrating this condition over the thickness of the top electrode and using Ohm's law (13) yields:

$$\boldsymbol{\nabla}_s u_1 \cdot \boldsymbol{n}_b = 0 \qquad \text{on } \Gamma \backslash \Gamma_1 \,. \tag{16}$$

The same holds for the bottom electrode, and the full set of boundary conditions is finally the same as in the case of the model based on transmission line theory, given by Eqs. (4).

3.4. Comparison between Maxwell and transmission line models

The equations governing the voltage distribution on resistive DE membranes have been derived using two methods: either by applying the transmission line theory which gives equations (2), or by using directly Maxwell's equations which yields equations (14). In both cases, the boundary conditions are the same and are given by equations (4).

If the dielectric membrane is at rest, $\boldsymbol{v} = 0$, and ϵ/h can be moved out of the derivative in equation (14). Equations (2) and (14) are then identical.

However, if the membrane moves and deforms, the voltage distribution appears to be coupled to the membrane movement, and equations (2) and (14) differ by the convective term $\boldsymbol{\nabla}_s \cdot \left(\epsilon/h(u_1 - u_2)\boldsymbol{v}_{\parallel}\right)$ in equation (14). This term matters when there is an in-plane movement of the membrane.

3.5. Linearization

We now consider that the actuator is driven by an oscillating voltage with a static bias: $u_a(t) = U + \tilde{u}_a(t)$, as it is often the case for DE actuators [27]. Equations (14) are linearized, by considering small voltage and displacement perturbations around a steady state:

$$u_1 = U + \tilde{u}_1(t), \qquad u_2 = 0 + \tilde{u}_2(t), \tag{17}$$

$$h = H + \tilde{h}(t), \qquad h_e = H_e + \tilde{h}_e(t). \tag{18}$$

Also, given the small thickness of the electrodes and of the membrane, it is assumed that the tangential velocity is the same in the whole membrane, meaning that $\boldsymbol{v}_{1\parallel} = \boldsymbol{v}_{2\parallel} = \boldsymbol{v}_{\parallel}$. The top and bottom electrode thicknesses and resistivity are also assumed to be identical and uniform along the thickness direction, which yields $\gamma_1 = \gamma_2 = h_e/r_e$.

The linearized versions of equations (14) are:

$$\begin{aligned}\frac{\epsilon}{H}\frac{\partial}{\partial t}\left(\tilde{u}_1 - \tilde{u}_2\right) - \frac{\epsilon U}{H^2}\frac{\partial \tilde{h}}{\partial t} =& \\ \boldsymbol{\nabla}_s \cdot \left(\frac{H_e}{r_e}\boldsymbol{\nabla}_s \tilde{u}_1\right) - U\boldsymbol{\nabla}_s \cdot \left(\frac{\epsilon}{H}\boldsymbol{v}_{\parallel}\right) \,,& \end{aligned} \tag{19a}$$

$$\begin{aligned}\frac{\epsilon}{H}\frac{\partial}{\partial t}\left(\tilde{u}_1 - \tilde{u}_2\right) - \frac{\epsilon U}{H^2}\frac{\partial \tilde{h}}{\partial t} =& \\ -\boldsymbol{\nabla}_s \cdot \left(\frac{H_e}{r_e}\boldsymbol{\nabla}_s \tilde{u}_2\right) - U\boldsymbol{\nabla}_s \cdot \left(\frac{\epsilon}{H}\boldsymbol{v}_{\parallel}\right) \,.& \end{aligned} \tag{19b}$$

Equations (19) show that even at first order, the voltage distribution is coupled to the mechanical vibrations, through the time derivative of the membrane thickness and through the membrane tangential velocity $\boldsymbol{v}_{\parallel}$. It must be noted that the coupling terms are proportional to the bias voltage U.

We emphasize that all effects which are discussed in the following are linear effects, independent of the

amplitude of the excitation. For larger excitation amplitudes, complex non-linear dynamics may arise, as studied in depth by other researchers e.g. [28, 29, 30], but are beyond the scope of the present article.

4. Experimental validation of the model

The model is now used to compute the mechanical and electrical behavior of the device shown in figure 1(a): an axisymmetric DE membrane inflated over a closed cavity.

The equations governing the dynamics of this membrane have already been derived [29, 21, 22, 31] and linearized around the inflated configuration. Appending equations (19) to the linearized dynamic equations results in a linear set of equations, which strongly couples electrical and mechanical dynamics. A weak form of these equations is built and solved in the frequency domain using the open source finite element solver FreeFEM (see [31, 22] for the details of the method).

Three calculations are compared to measurements in the following:

- *Model w/o resistance*: it is assumed that the electrodes are perfectly conductive, so the voltage is uniform on the electrodes for all frequencies, and equal to the applied voltage.
- *Uncoupled model*: the electrical diffusion equations (19) are solved first, assuming the geometry is static. The obtained frequency-dependent voltage distribution is then used as a given input to the mechanical calculation. This is the approach used by the authors who consider nonuniform voltage distributions on dielectric elastomers.
- *Coupled model*: the system of fully coupled electrical and mechanical equations is solved, meaning that the influence of the vibrations of the membrane on the voltage distribution is taken into account.

The parameters of the studied membrane are given in table 1. The behavior of the silicone membrane is modelled by a Gent hyperelastic law. The shear modulus μ and the stiffening parameter J_m are estimated by fitting a simulation of the quasistatic inflation of the membrane on an inflation experiment. The range of the pressure sensor that we used limited the achievable biaxial stretches to approximately 1.7, at which the stiffening of the elastomer is not very steep. As a consequence, the estimation of J_m is not very accurate, and explains the large value in table 1. However, all measurements presented in this article are obtained for relatively small strains, for which J_m has little influence.

Dissipation effects related to the viscosity of the elastomer are taken into account by structural damping, using a constant loss factor η in the membrane.

Table 1. Parameters of the studied prototype. The membrane and electrode thicknesses H_0 and H_{e0} are given in the reference configuration, before the membrane is pre-stretched and inflated.

Name	Symbol	Value
Shear modulus	μ	450 kPa
Gent stiffening parameter [32]	J_m	60
Material loss factor	η	2 %
Membrane thickness	H_0	50 µm
Electrode thickness	H_{e0}	2 µm
Electrode resistivity	r_e	0.5 Ωm
Membrane radius	A	19 mm
Membrane biaxial pre-stretch	λ_{pre}	1.1
Membrane density	ρ	1042 kg m^{-3}
Membrane relative permittivity	ϵ_r	2.8
Inflation pressure	P	1500 Pa
Bias voltage	U	1500 V
Oscillating voltage amplitude	$\lvert\tilde{u}_a\rvert$	20 V

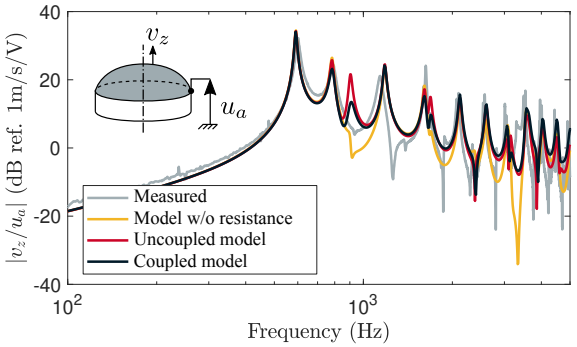

Figure 4. Transfer function between the vertical velocity of the membrane v_z at radius $R = 0.1 \times A$ and the applied voltage, measured using a laser vibrometer and computed.

To assess the performance of the model and of the numerical implementation, the membrane is excited with white noise, and its velocity is measured using a laser vibrometer (Polytec PSV-500). The transfer function between the applied voltage and the velocity is obtained using the H_1 transfer function estimate [33], and plotted in figure 4 together with the numerical results.

The *Model w/o resistance*, *Coupled model* and *Uncoupled model* differ most largely around the third membrane mode, at 900 Hz. The coupled model yields a larger loss factor for the third mode, indicating that some mechanical energy is transferred to the electrical part of the system and is dissipated by resistive effects. All three models provide a convincing estimation of the dynamics of the system, which suggest that for the considered electrode resistivity the coupling between the vibrations and the voltage distribution has a minor effect on the electrostatic excitation. To further analyse the consequences of this coupling, the electrical behavior of the inflated membrane is now analysed.

The impedance of the membrane u_a/i can be obtained from the numerical results, as the current flowing through the membrane Σ reads:

$$i = \int_\Sigma \frac{\epsilon}{H}\frac{\partial}{\partial t}(\tilde{u}_1 - \tilde{u}_2)dS + \int_\Sigma \epsilon U \frac{\partial}{\partial t}\left(\frac{1}{\tilde{h}}\right) dS \,. \qquad (20)$$

In figure 5, this computed impedance is compared to the measured impedance, obtained using the current measured in a shunt resistor and the voltage given by the monitor output of the Trek 609-E amplifier used for the experiments.

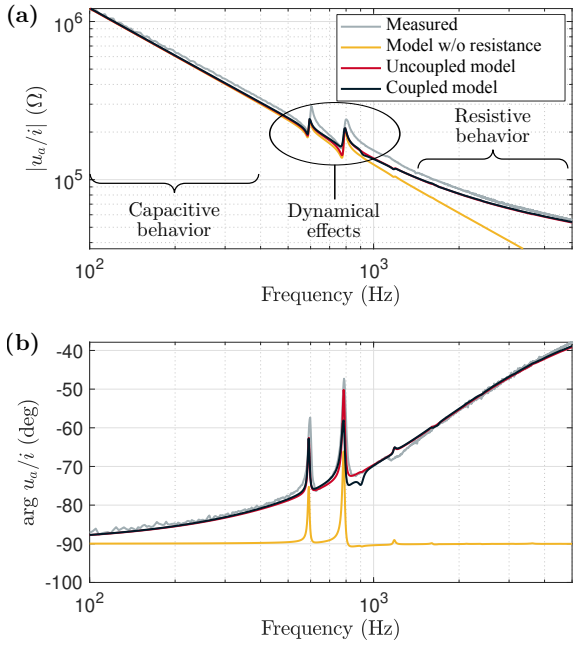

Figure 5. Membrane impedance, measured on a prototype, and computed with the *Model w/o resistance*, *Uncoupled model* and *Coupled model*. **(a)** Amplitude. **(b)** Phase.

The $1/\omega$ behavior of the impedance at low frequencies (below 500 Hz) is characteristic of a capacitor, and resistive effects make it deviate from the capacitive behavior at high frequencies. As the frequency of the excitation passes one of the first eigenfrequencies of the membrane, a large displacement will be caused by the applied voltage u_a. As a consequence, the membrane thickness will oscillate, and the second term in (20) results in peaks in the impedance, which are both measured and computed by the three models. The impedance thus reveals coupling effects between the electrodynamic loading of the membrane and its vibrations. This coupling mechanism is not related to the electrode resistivity, but to capacitance changes during actuation, and occurs even with perfectly conductive electrodes (*model w/o resistance*). It can thus be described by models which assume a uniform voltage on the electrodes.

The measurement of the impedance may provide useful information for self-sensing, as the first membrane eigenfrequencies for example can be estimated only from impedance measurements by peak-picking algorithms. This information can then be used to perform adaptive filtering for example.

Here again, figure 5 shows that there are only very small differences between the results of the *Coupled model* and *Uncoupled model*, and the comparison with the measurements does not show that the prediction of the coupled model is better.

The voltage on the electrodes is now investigated, and the usefulness of the coupled model is demonstrated. The voltage is measured using a high voltage probe, as explained in figures 1(a) and 1(b). The electrode voltage u_1 is measured at different radii, and plotted in figure 6, together with the results of the models.

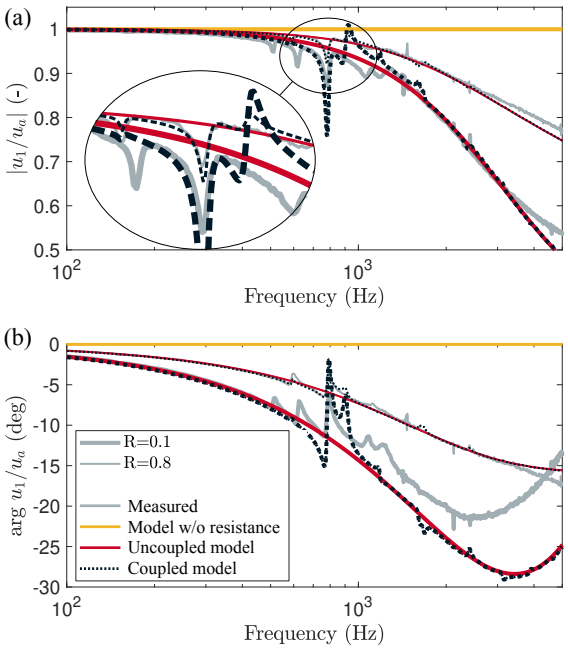

Figure 6. Transfer function between the voltage on the top electrode u_1 at different radii during actuation and the applied voltage u_a, measured and computed. **(a)** Amplitude. **(b)** Phase.

On the one hand, the *model w/o resistance* assumes that the voltage is uniform on the electrodes, and equal to the applied voltage. As a consequence, it is not able to describe the measured frequency dependence. On the other hand, both the *Uncoupled model* and the *Coupled model* capture the decrease of the voltage at high frequencies due to electrode resistivity. The further away from the electrical the connections the measurement point is located, the faster the voltage decreases at high frequencies. This result is well known and has been analysed by transmission line models on DEs [12, 13, 11].

What is more interesting is the behavior of the

voltage on the electrodes at medium frequencies, around 1 kHz. Peaks and drops are observed at the membrane eigenfrequencies, as already analysed in figure 1. These peaks are caused by the coupling between the membrane vibrations and the voltage diffusion, through the coupling terms which appear in equation (19). Indeed, the *Uncoupled model* which does not take these terms into account is not able to predict the observed peaks. The *Coupled model* on the other hand gives a good estimation of the drop at 800 Hz for example. The errors between the model and the experiments on the other peaks and drops may be related to errors in the calculation of the dynamics (see figure 4) or to measurement errors. Indeed, the measurement of the voltage on a vibrating membrane at high frequencies is difficult (see figure 1), as any connecting wire tends to interfere with the dynamics.

To conclude this section, the voltage distribution on the electrodes of vibrating DEAs is influenced by the membrane movement, and it has been shown that this effect arises from the coupling terms in equation (19). The physical origin of the coupling will be discussed in the following section.

5. Discussion

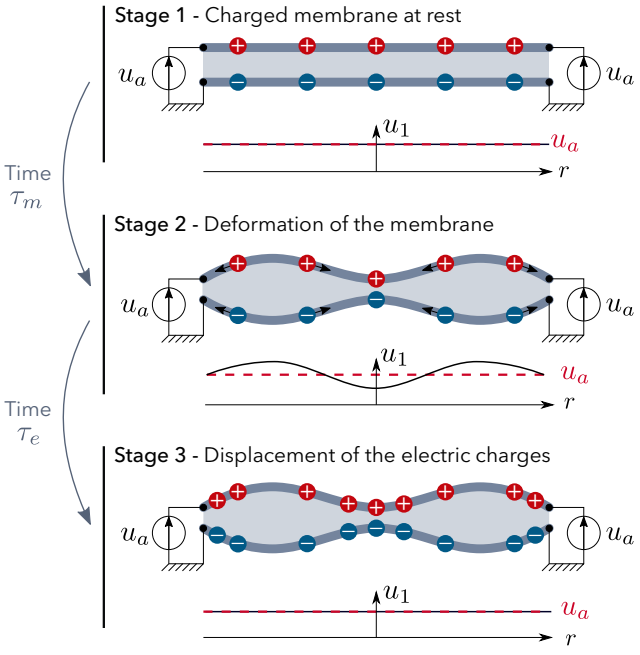

Figure 7. Physical interpretation of the observed coupling mechanism. The characteristic times of electrical and mechanical effects are τ_e and τ_m, respectively. The distinction between the three stages is made here for pedagogical reasons, and does not occur in practice.

In this section, the coupling observed in figure 6 and its consequences are discussed.

The peaks in the voltage at the membrane eigenfrequencies seen in figure 6 can be explained by figure 7 where the dynamic loading of a membrane is decomposed into three stages:

- **Stage 1** Consider a DE membrane at rest, charged by a static voltage at its edge.
- **Stage 2** Suppose that, under external action, the membrane deforms during a mechanical response time τ_m. This deformation induces local changes in thickness. Before the charges move on the membrane, due to Gauss's law (12) the voltage on the membrane will increase where it is thicker, and decrease where it is thinner.
- **Stage 3** Charges will be supplied by the generator, and they will move on the membrane so that the voltage equals the applied voltage everywhere. This diffusion occurs during the timescale τ_e.

In practice, the membrane is actuated by a non stationary input voltage $u_a(t)$, which vibrates the system at the period τ_m. The deformation is most significant at system's eigenmodes, thus, we now examine the case where the excitation frequency matches one of the eigenfrequencies. The electromechanical behavior of the system is governed by the ratio of the mechanical timescale τ_m and the electrical time τ_e. Note that for such a resonant system, the mechanical timescale is dictated by the system's resonances, and not by the material viscoelastic relaxation time constants.

- If $\tau_e \ll \tau_m$, the electrodynamic equilibrium is satisfied at all times, the voltage is uniform on the membrane, and equal to the applied voltage $u_a(t)$.
- If $\tau_e \approx \tau_m$, the charge diffusion takes approximately one period of oscillation, so the electrostatic equilibrium is not satisfied at all times. There are locally excess charges which generate voltage fluctuations, and the coupling phenomenon described in figure 7 then occurs.
- If $\tau_e \gg \tau_m$, the charges do not have the time to spread on the membrane, so the electrostatic excitation is small, and the membrane does not move. If the membrane is vibrated by another mechanical excitation of period τ_m, the voltage will still locally vary on the electrodes because the charges are 'fixed' by the high resistivity.

For the current prototype, the time scales for the charge diffusion effects τ_e and for the mechanical effects τ_m can be estimated by:

$$\tau_e = \frac{\epsilon A^2 r_e}{H H_e} \approx 50\,\mu\text{s}\,, \quad \tau_m = \frac{A}{\sqrt{\mu/\rho}} \approx 900\,\mu\text{s}\,, \quad (21)$$

with the parameters defined in table 1. There is a difference in the order of magnitude between τ_e and τ_m of about 20, and the coupling is still visible. It is however expected that it would be even stronger with more resistive electrodes, which would increase τ_e.

To have an insight of the consequences of this coupling for higher resistivity electrodes, we use the model to compute the voltage distribution on the inflated membrane at 1179 Hz, which corresponds to the fourth membrane eigenfrequency. The results are plotted in figure 8.

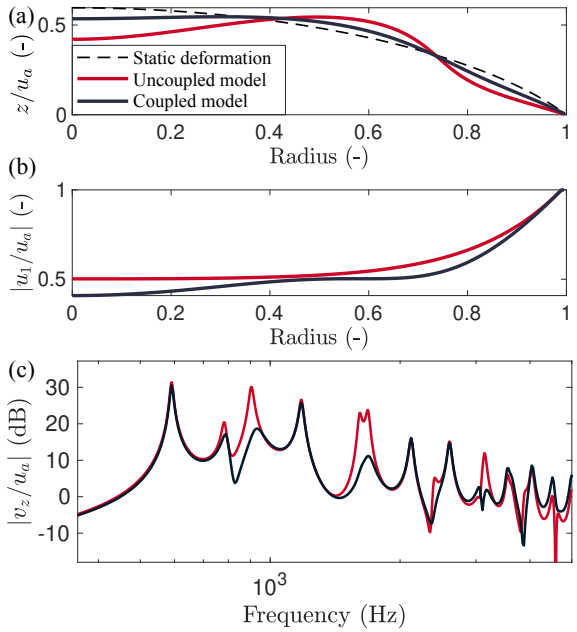

Figure 8. Computed dynamics of the inflated DE membrane at the fourth eigenfrequency 1179 Hz, for more resistive electrodes ($\tau_m/\tau_e = 5$). (a) Vertical position z of the static deformation of the membrane and of the operational deflection shape around the static equilibrium, scaled so that the maximum displacement of the *Uncoupled model* is 0.3. The same scaling is used for both calculations. (b) Voltage distribution at 1179 Hz, obtained with the *Uncoupled model* and the *Coupled model*. (c) Transfer function between the normal velocity at the center of the membrane v_z and the excitation voltage u_a.

Figure 8(b) shows that the voltage distribution on the membrane is influenced by the membrane dynamics, as the results of the *Uncoupled model* and *Coupled model* differ. The voltage on the electrodes oscillates with a wavelength which is similar to the mechanical wavelength which can be observed in figure 8(a). This suggests that information on the local deformation of the membrane at high frequencies can be obtained by voltage measurements on the electrodes, which could be useful for self-sensing. Moreover, figure 8(c) indicates that for more resistive electrodes than the measured ones (see figure 4), the *Coupled model* ans *Uncoupled model* differ more, which suggests that for highly resistive electrodes it is necessary to take into account the coupling between the vibrations and the voltage distribution to compute accurately the electrostatic excitation. Experimental studies with more resistive electrodes would provide further insights in this direction.

6. Conclusion

To conclude, the present article provides an analysis of resistivity effects on dielectric elastomers. It has been shown experimentally that for a certain set of parameters, when the timescale for electrodynamics is similar to the mechanical timescale, a coupling between the voltage distribution and the vibrations of the membrane occurs.

The equations governing the voltage distribution on moving resistive dielectric elastomer membranes have been derived, and linearized around a pre-stressed configuration with a static bias voltage. The linear model succeeds in describing the observed coupling.

When the electrode resistivity is high, it is necessary to take into account the influence of the membrane dynamics on the voltage to compute accurately the electrostatic excitation on the membrane. The proposed model therefore refines the modelling of the excitation in resistive dielectric elastomer actuators. In practice, this may typically happen for example for DE loudspeakers [34, 35, 36], which operate at high frequencies, or for DE devices with resistive electrodes driven at lower frequencies.

The studied coupling also opens self-sensing possibilities, as information on the membrane dynamics can be deduced from voltage and impedance measurements. More precisely, the local variations of the voltage on the electrodes provides information on the local deformation. This may lead to self-sensing applications to control dielectric elastomer actuators operated at high frequencies, where the standard capacitive sensing approaches no longer work, as the membrane thickness varies locally, and no longer in a uniform way.

Preliminary experimental investigations have been conducted to demonstrate the coupling, but we believe that dedicated experiments with even more resistive electrodes would help understanding the possible applications, especially for self sensing.

Acknowledgments

The authors thank Bekir Aksoy and Herbert Shea from the EPFL for the help in manufacturing the prototype. The authors acknowledge the support of the French National Research Agency within the project SMArT (ANR-15-CE08-0007-02).

Appendix A. Integration of electrodynamic equations

In this appendix Maxwell's equations are integrated in the normal direction in order to obtain surface equations.

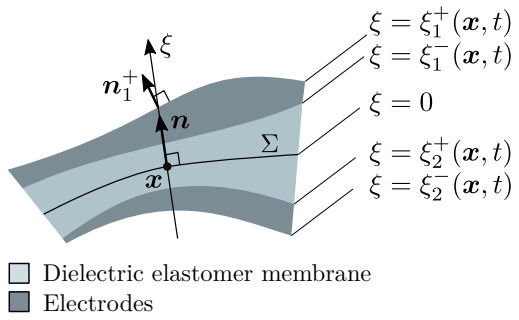

Figure A1. Definition of the geometry of a thin membrane for the simplification of Maxwell's equations. A point of the system is identified by the location $\boldsymbol{x}$ of its projection on the reference surface, and its coordinate ξ along the normal $\boldsymbol{n}$ to the reference surface. Surfaces $\xi = \xi_i^{\pm}(\boldsymbol{x},t)$ define the bottom and top sides of the electrodes, so that the thickness of the dielectic membrane is $h = \xi_1^- - \xi_2^+$, and the thicknesses of the top and bottom electrodes are $\xi_1^+ - \xi_1^-$ and $\xi_2^+ - \xi_2^-$ respectively, both supposed to be equal to h_e in the section 3.2.

Each point in the volume of the membrane is identified by a point $\boldsymbol{x}$ on the reference surface and an altitude ξ, see figure A1. For an arbitrary vector field $\boldsymbol{a}(\boldsymbol{x},\xi)$ in this volume, $\boldsymbol{a}_\parallel(\boldsymbol{x},\xi)$ denotes its projection on the tangent plane to the reference surface at location $\boldsymbol{x}$.

The equations will be expressed using surface operators: the notation $\boldsymbol{\nabla}_s a$ refers to the surface gradient of a scalar field a, defined as the projection of $\boldsymbol{\nabla} a$ on the tangent plane to the reference surface, and $\boldsymbol{\nabla}_s \cdot \boldsymbol{a}$ refers to the surface divergence of a vector field $\boldsymbol{a}$, defined as the divergence of $\boldsymbol{a}_\parallel$. Assuming that the thickness of the membrane is much smaller than the radius of curvature of the reference surface, the following relation holds:

$$\boldsymbol{\nabla} = \boldsymbol{\nabla}_s + \frac{\partial}{\partial \xi}\boldsymbol{n} \,. \tag{A.1}$$

Appendix A.1. Integration of Gauss's law

Using Eq. (A.1), the integration of Gauss's law (6a) from the reference surface to the outer boundary of the top electrode reads:

$$\int_0^{\xi_1^+} \boldsymbol{\nabla}_s \cdot \boldsymbol{D} \mathrm{d}\xi + \int_0^{\xi_1^+} \frac{\partial \boldsymbol{D}}{\partial \xi}\mathrm{d}\xi \cdot \boldsymbol{n} = \int_0^{\xi_1^+} \rho \mathrm{d}\xi \,. \tag{A.2}$$

Note that the interval of integration includes the interface where $\boldsymbol{D}\cdot\boldsymbol{n}$ was assumed to be discontinuous. The jump of $\boldsymbol{D}$, related to the charge density ρ, is expressed by the second member. Given that there are charges only in the electrode, Eq. (A.2) is then rewritten as:

$$\int_0^{\xi_1^+} \boldsymbol{\nabla}_s \cdot \boldsymbol{D} \mathrm{d}\xi - D_\perp = \sigma \,, \tag{A.3}$$

where σ is the surface charge density of the top electrode defined as:

$$\sigma = \int_{\xi_1^-}^{\xi_1^+} \rho \mathrm{d}\xi \,, \tag{A.4}$$

and $D_\perp$ is the normal component of the electric displacement in the membrane, which does not depend on ξ as seen in Eqs. (9) and (10). The normal component of the electric field in the membrane is much larger than its tangential component both in the electrode and in the membrane and, in addition, the membrane radius is much larger that its thickness so the first term of Eq. (A.3) is negligible compared to the second one. Finally, combining Eqs. (A.3), (9) and (10) gives the expression of the surface charge density as a function of the electrode potentials Eq. (12).

The same procedure applied to the bottom electrode shows that its surface charge density is $-\sigma$.

Appendix A.2. Integration of the charge balance

Integrating the charge balance equation (6b) over the thickness of the top electrode reads:

$$\int_{\xi_1^-}^{\xi_1^+} \boldsymbol{\nabla}_s \cdot \boldsymbol{i} \mathrm{d}\xi + \left(\int_{\xi_1^-}^{\xi_1^+} \frac{\partial \boldsymbol{i}}{\partial \xi}\mathrm{d}\xi\right) \cdot \boldsymbol{n} + \int_{\xi_1^-}^{\xi_1^+} \frac{\partial \rho}{\partial t}\mathrm{d}\xi = 0 \,. \tag{A.5}$$

Using the Leigniz integral rule to express the terms of this equation yields:

$$\begin{aligned} \boldsymbol{\nabla}_s \cdot \left(\int_{\xi_1^-}^{\xi_1^+} \boldsymbol{i} \mathrm{d}\xi\right) &- \boldsymbol{i}(\xi_1^+) \cdot \left(\boldsymbol{\nabla}_s \xi_1^+ - \boldsymbol{n}\right) \\ &+ \boldsymbol{i}(\xi_1^-) \cdot \left(\boldsymbol{\nabla}_s \xi_1^- - \boldsymbol{n}\right) + \frac{\partial}{\partial t}\left(\int_{\xi_1^-}^{\xi_1^+} \rho \mathrm{d}\xi\right) \\ &- \rho(\xi_1^+)\frac{\partial \xi_1^+}{\partial t} + \rho(\xi_1^-)\frac{\partial \xi_1^-}{\partial t} = 0 \,. \end{aligned} \tag{A.6}$$

As neither the dielectric membrane nor the surrounding air can conduct free charges, the boundary conditions for the current on the top and bottom surfaces of the electrode read $\boldsymbol{i}'(\xi_1^\pm) \cdot \boldsymbol{n}_1^\pm = 0$, that is:

$$\left[\boldsymbol{i}(\xi_1^\pm) - \rho(\xi_1^\pm)\boldsymbol{v}(\xi_1^\pm)\right] \cdot \left(\boldsymbol{n} - \boldsymbol{\nabla}_s \xi_1^\pm\right) = 0 \,. \tag{A.7}$$

Moreover, the normal velocity of the interfaces reads:

$$\boldsymbol{v}(\xi_1^\pm) \cdot \boldsymbol{n} = \frac{\partial \xi_1^\pm}{\partial t} + \boldsymbol{v}(\xi_1^\pm) \cdot \boldsymbol{\nabla}_s \xi_1^\pm \,, \tag{A.8}$$

so the boundary conditions (A.7) become:

$$\boldsymbol{i}(\xi_1^{\pm}) \cdot \left(\boldsymbol{n} - \boldsymbol{\nabla}_s \xi_1^{\pm}\right) - \rho(\xi_1^{\pm}) \frac{\partial \xi_1^{\pm}}{\partial t} = 0 \; . \tag{A.9}$$

Introducing these boundary conditions in the charge balance (A.6) cancels all the boundary terms, so this equation finally gives Eq. (11), where σ is the surface charge density defined by Eq. (A.4), and the surface current density on the top electrode

$$\boldsymbol{j}_1 = \int_{\xi_1^-}^{\xi_1^+} \boldsymbol{i}_{\parallel} \mathrm{d}\xi \; , \tag{A.10}$$

has been introduced.

Appendix A.3. Integration of Ohm's law

In this work, we are interested in the voltage distribution on the electrodes, which is related to the charges' in-plane motion. The slowing down of this motion, due to the resistivity of the electrodes, is described by Ohm's law. Since the significant component of the charges' motion is the tangential one, Ohm's law (8) is projected on the tangent plane to the reference surface:

$$\boldsymbol{i}_{\parallel} - \rho \boldsymbol{v}_{\parallel} = \frac{1}{r_e} \boldsymbol{E}_{\parallel} \; . \tag{A.11}$$

As in the precedent paragraphs, let us examine the case of the top electrode. The electric field is there given by the surface gradient of the potential u_1 and is uniform in the electrode thickness. Integrating Eq. (A.11) over the electrode thickness yields:

$$\int_{\xi_1^-}^{\xi_1^+} \boldsymbol{i}_{\parallel} \mathrm{d}\xi - \int_{\xi_1^-}^{\xi_1^+} \rho \boldsymbol{v}_{\parallel} \mathrm{d}\xi = -\boldsymbol{\nabla}_s u_1 \int_{\xi_1^-}^{\xi_1^+} \frac{1}{r_e} \mathrm{d}\xi \; . \tag{A.12}$$

In order to recognize in the second term the surface charge σ defined by Eq. (A.4), we further assume that the tangential velocity $\boldsymbol{v}_{\parallel}$ does not depend on ξ in the electrodes. This tangential velocity is denoted by $\boldsymbol{v}_{1\parallel}$ and $\boldsymbol{v}_{2\parallel}$ in the top and bottom electrodes respectively. The surface Ohm's law (A.12) is then simplified to yield Eq. (13), where $\boldsymbol{j}_1$ is the surface current defined by Eq. (A.10), and the surface conductivity of the top electrode

$$\gamma_1 = \int_{\xi_1^-}^{\xi_1^+} \frac{1}{r_e} \mathrm{d}\xi \; , \tag{A.13}$$

has been introduced.

References

[1] Ron Pelrine, Roy Kornbluh, Qibing Pei, and Jose Joseph. High-Speed Electrically Actuated Elastomers with Strain Greater Than 100%. *Science*, 287(5454):836–839, February 2000.

[2] Yu Feng Goh, Samin Akbari, Tran Vy Khanh Vo, and Soo Jin Adrian Koh. Electrically-Induced Actuation of Acrylic-Based Dielectric Elastomers in Excess of 500% Strain. *Soft Robotics*, 5(6):675–684, December 2018.

[3] Samuel Rosset, Benjamin M O'Brien, Todd Gisby, Daniel Xu, Herbert R Shea, and Iain A Anderson. Self-sensing dielectric elastomer actuators in closed-loop operation. *Smart Materials and Structures*, 22(10):104018, October 2013.

[4] Kwangmok Jung, Kwang J. Kim, and Hyouk Ryeol Choi. A self-sensing dielectric elastomer actuator. *Sensors and Actuators A: Physical*, 143(2):343–351, May 2008.

[5] Weili Hu, Xiaofan Niu, Ran Zhao, and Qibing Pei. Elastomeric transparent capacitive sensors based on an interpenetrating composite of silver nanowires and polyurethane. *Applied Physics Letters*, 102(8):083303, February 2013.

[6] Todd A. Gisby, Benjamin M. O'Brien, and Iain A. Anderson. Self sensing feedback for dielectric elastomer actuators. *Applied Physics Letters*, 102(19):193703, May 2013.

[7] Peter Sommer-Larsen, Jacob C. Hooker, Guggi Kofod, Keld West, Mohammed Benslimane, and Peter Gravesen. Response of dielectric elastomer actuators. In Yoseph Bar-Cohen, editor, *SPIE's 8th Annual International Symposium on Smart Structures and Materials*, page 157, Newport Beach, CA, USA, July 2001.

[8] N. C. Goulbourne, E. M. Mockensturm, and M. I. Frecker. Electro-elastomers: Large deformation analysis of silicone membranes. *International Journal of Solids and Structures*, 44(9):2609–2626, May 2007.

[9] Christoph Keplinger, Martin Kaltenbrunner, Nikita Arnold, and Siegfried Bauer. Capacitive extensometry for transient strain analysis of dielectric elastomer actuators. *Applied Physics Letters*, 92(19):192903, May 2008.

[10] Daniel Xu, Silvain Michel, Thomas McKay, Benjamin O'Brien, Todd Gisby, and Iain Anderson. Sensing frequency design for capacitance feedback of dielectric elastomers. *Sensors and Actuators A: Physical*, 232:195–201, August 2015.

[11] Daniel Xu, Andreas Tairych, and Iain A Anderson. Stretch not flex: Programmable rubber keyboard. *Smart Materials and Structures*, 25(1):015012, January 2016.

[12] W. Kaal, S. Herold, and T. Melz. Modeling approaches for electroactive polymers. In Yoseph Bar-Cohen, editor, *SPIE Smart Structures and Materials + Nondestructive Evaluation and Health Monitoring*, page 764211, San Diego, California, USA, March 2010.

[13] Christian Graf and Jürgen Maas. In-Plane Field Propagation in EAP Transducers Based on the Equivalent Network Method. In *Volume 1: Development and Characterization of Multifunctional Materials; Modeling, Simulation and Control of Adaptive Systems; Structural Health Monitoring*, page 207, Stone Mountain, Georgia, USA, September 2012. ASME.

[14] Thorben Hoffstadt, Philip Meier, and Jürgen Maas. Modeling Approach for the Electrodynamics of Multilayer DE Stack-Transducers. In *Volume 1: Multifunctional Materials; Mechanics and Behavior of Active Materials; Integrated System Design and Implementation; Structural Health Monitoring*, page V001T02A015, Stowe, Vermont, USA, September 2016. ASME.

[15] Thorben Hoffstadt and Jürgen Maas. Self-Sensing Control for Soft-Material Actuators Based on Dielectric Elastomers. *Frontiers in Robotics and AI*, 6, 2019.

[16] G Rizzello, M Hodgins, D Naso, A York, and S Seelecke. Modeling of the effects of the electrical dynamics on the electromechanical response of a DEAP circular actuator with a mass–spring load. *Smart Materials and Structures*, 24(9):094003, September 2015.

[17] G Rizzello, D Naso, A York, and S Seelecke. Closed loop control of dielectric elastomer actuators based on self-sensing displacement feedback. *Smart Materials and Structures*, 25(3):035034, March 2016.

[18] Kimberly Pope, Alyson Tews, Mary I. Frecker, Eric Mockensturm, Nakhiah C. Goulbourne, and Alan J. Snyder. Dielectric elastomer laminates for active membrane pump applications. In *Smart Structures and Materials 2004: Electroactive Polymer Actuators and Devices (EAPAD)*, volume 5385, pages 60–68. International Society for Optics and Photonics, July 2004.

[19] Naoki Hosoya, Hiroaki Masuda, and Shingo Maeda. Balloon dielectric elastomer actuator speaker. *Applied Acoustics*, 148:238–245, May 2019.

[20] Richard Heydt, Ron Pelrine, Jose Joseph, Joseph Eckerle, and Roy Kornbluh. Acoustical performance of an electrostrictive polymer film loudspeaker. *The Journal of the Acoustical Society of America*, 107(2):833–839, 2000.

[21] J. W. Fox and N. C. Goulbourne. Electric field-induced surface transformations and experimental dynamic characteristics of dielectric elastomer membranes. *Journal of the Mechanics and Physics of Solids*, 57(8):1417–1435, August 2009.

[22] Emil Garnell, Corinne Rouby, and Olivier Doaré. Dynamics and sound radiation of a dielectric elastomer membrane. *Journal of Sound and Vibration*, 459:114836, October 2019.

[23] Samuel Rosset, Oluwaseun A. Araromi, Samuel Schlatter, and Herbert R. Shea. Fabrication Process of Silicone-based Dielectric Elastomer Actuators. *Journal of Visualized Experiments : JoVE*, (108), February 2016.

[24] C Graf and J Maas. A model of the electrodynamic field distribution for optimized electrode design for dielectric electroactive polymer transducers. *Smart Materials and Structures*, 21(9):094001, September 2012.

[25] A. Kovetz. *Electromagnetic Theory*. Oxford University Press, Oxford, New York, March 2000.

[26] Ursula van Rienen, Jürgen Flehr, Ute Schreiber, and Victor Motrescu. Modeling and Simulation of Electro-Quasistatic Fields. In Kurt Antreich, Roland Bulirsch, Albert Gilg, and Peter Rentrop, editors, *Modeling, Simulation, and Optimization of Integrated Circuits*, ISNM International Series of Numerical Mathematics, pages 17–31. Birkhäuser Basel, 2003.

[27] Takehiro Sugimoto, Kazuho Ono, Akio Ando, Yuichi Morita, Kosuke Hosoda, and Daisaku Ishii. Semicylindrical acoustic transducer from a dielectric elastomer film with compliant electrodes. *The Journal of the Acoustical Society of America*, 130(2):744–752, 2011.

[28] Jian Zhu, Shengqiang Cai, and Zhigang Suo. Nonlinear oscillation of a dielectric elastomer balloon. *Polymer International*, 59(3):378–383, March 2010.

[29] Jian Zhu, Shengqiang Cai, and Zhigang Suo. Resonant behavior of a membrane of a dielectric elastomer. *International Journal of Solids and Structures*, 47(24):3254–3262, December 2010.

[30] Chongjing Cao, Thomas L. Hill, Bo Li, Lei Wang, and Xing Gao. Nonlinear dynamics of a conical dielectric elastomer oscillator with switchable mono to bi-stability. *International Journal of Solids and Structures*, page S0020768320300512, February 2020.

[31] Emil Garnell, Olivier Doaré, and Corinne Rouby. Coupled vibro-acoustic modeling of a dielectric elastomer loudspeaker. *The Journal of the Acoustical Society of America*, 147(3):1812–1821, March 2020.

[32] A. N. Gent. A New Constitutive Relation for Rubber. *Rubber Chemistry and Technology*, 69(1):59–61, March 1996.

[33] David J Ewins. *Modal Testing: Theory and Practice*, volume 15. Research studies press Letchworth, 1984.

[34] Richard Heydt, Roy Kornbluh, Joseph Eckerle, and Ron Pelrine. Sound radiation properties of dielectric elastomer electroactive polymer loudspeakers. In *Smart Structures and Materials 2006: Electroactive Polymer Actuators and Devices (EAPAD)*, volume 6168, page 61681M, San Diego, California, USA, March 2006. International Society for Optics and Photonics.

[35] Naoki Hosoya, Shun Baba, and Shingo Maeda. Hemispherical breathing mode speaker using a dielectric elastomer actuator. *The Journal of the Acoustical Society of America*, 138(4):EL424–EL428, October 2015.

[36] Christoph Keplinger, Jeong-Yun Sun, Choon Chiang Foo, Philipp Rothemund, George M. Whitesides, and Zhigang Suo. Stretchable, Transparent, Ionic Conductors. *Science*, 341(6149):984–987, August 2013.